Carbon Nanotubes

DOI: 10.1002/ange.201304032

Stable Electron Donor–Acceptor Nanohybrids by Interfacing *n*-Type TCAQ with *p*-Type Single-Walled Carbon Nanotubes**

Carlos Romero-Nieto, Raúl García, María Ángeles Herranz, Laura Rodríguez-Pérez, Macarena Sánchez-Navarro, Javier Rojo, Nazario Martín, and Dirk M. Guldi**

Since the discovery by S. Iijima in 1991,[1] an entire area of research has focused on the chemistry of 1D nanocarbons, namely carbon nanotubes (CNTs), in general, and single-walled carbon nanotubes (SWCNTs), in particular.[2,3] They exhibit unique properties and as such have found their way into diverse emerging fields.[4] These properties are, however, only discernible for single-walled carbon nanotubes that are debundled, individualized, and stabilized in, for example, solution.[5] In this respect, to improve the poor solubility of SWCNTs and to realize their full potential, the covalent and noncovalent modifications of single-walled carbon nanotubes have emerged as powerful approaches.[2]

In particular, the paradigm is shifting towards optimizing noncovalent interactions since they assist in improving the solubility without altering the electronic structure of SWCNTs, especially in terms of conductivity.[6] Considering, for example, the intrinsic nature of SWCNTs, namely *p*-type, complementing them with the right *n*-type building block is crucial, especially within the context of dispersability and stability of the resulting electron donor–acceptor nanohybrids. This concept has recently been corroborated by means of immobilizing *n*-type amphiphilic perylenebisdiimides,[7,8] and *n*-type phenylenevinylene oligomers[9,10] in water and organic solvents, respectively. In addition to charge-transfer interactions (i.e., *n*-/*p*-type), π–π stacking and hydrophobic forces are essential to adjust the stability. None of these built, however, on the effect of multiple *n*-type building blocks. Only *p*-type building blocks in the form of extended tetrathiafulvalene (exTTF) have recently been explored.[11] To this end, nanotweezers of exTTF combine the synergy of π–π stacking, concave–convex complementarity, and/or electron donor–acceptor interactions with SWCNTs, with a versatile second generation dendron that carries terminal carboxylic groups. Most importantly, the electronic communication between semiconducting SWCNTs, on one hand, and the water-soluble exTTF nanotweezers, on the other hand, has been demonstrated to result from efficient immobilization by means of noncovalent interactions.[11a]

Turning to *n*-type building blocks, 11,11,12,12-tetracyano-9,10-anthraquinodimethane (TCAQ) has been employed in the current study as the electron acceptor of choice owing to its remarkable electronic and geometrical features.[12] In particular, TCAQs exhibit low reduction potentials and high stabilities of the reduced species because of the aromatization of the central quinoid moiety. In the reduced form, the charge is efficiently spread over the two dicyanomethylenes and the central anthracene affording highly stabilized radical anion and dianion species.[13] Notably, the concave feature of neutral TCAQ complements the convex structure of SWCNTs and, as such, provides the means for sizeable electronic communication based on, for example, hydrophobic interactions, π–π interactions, and charge-transfer interactions.[14] Finally, choosing a nanotweezer geometry enables augmenting the aforementioned forces owing to the benefits that stem from the synergy of two TCAQs and their concave–convex complementarity with SWCNTs.

We focused therefore our attention on the design, synthesis, and probing of versatile TCAQ nanotweezers that, despite their low degree of preorganization, immobilize onto SWCNTs and, in turn, *p*-type dope the SWCNTs in solution. Notably, we have also been diligent with the choice of SWCNTs using the patented CoMoCAT process. In particular, to dissect the impact on the charge separation and charge recombination kinetics, we tested and compared different CoMoCAT SWCNTs including samples that are mixtures of different chiralities (i.e., mixed CoMoCAT) as well as enriched SWCNTs (i.e., (6,5) and (7,6)). As a matter of fact, the synergy of myriad forces leads to an unprecedented stability for SWCNT-based nanohybrids and to chirality-dependent photophysics.

The solubility of TCAQs in aqueous media was ensured by peripheral derivatization with a dendron that allows the incorporation of eight carboxylic acids in the resulting TCAQ nanotweezers (**1**). Full details about the syntheses and

[*] Dr. C. Romero-Nieto, Prof. Dr. D. M. Guldi
Friedrich-Alexander-Universität Erlangen-Nürnberg
Department of Chemistry and Pharmacy & Interdisciplinary Center for Molecular Materials (ICMM)
Egerlandstrasse 3, 91058 Erlangen (Germany)
E-mail: dirk.guldi@chemie.uni-erlangen.de
Dr. R. García, Dr. M. A. Herranz, Dr. L. Rodríguez-Pérez, Prof. Dr. N. Martín
Departamento de Química Orgánica I, Facultad de Química
Universidad Complutense, 28040 Madrid (Spain)
E-mail: nazmar@quim.ucm.es
Prof. Dr. N. Martín
IMDEA-Nanociencia
Campus Cantoblanco, 28049 Madrid (Spain)
Dr. M. Sánchez-Navarro, Dr. J. Rojo
Glycosystems Laboratory, Instituto de Investigaciones Químicas
CSIC-Universidad de Sevilla
Américo Vespucio, 49, Isla de la Cartuja 41092 Sevilla (Spain)

[**] Financial support from MINECO of Spain (grant numbers CTQ2011-24652, PIB2010JP-00196, 2010C-07-25200, and Consolider-Ingenio CSD2007-00010), FUNMOLS (grant number FP7-212942-1), CAM (grant number MADRISOLAR-2 S2009/PPQ-1533), DFG (grant number GU 517/16-1), and DFG (Excellence Cluster—Engineering of Advanced Materials) is greatly appreciated.
TCAQ = 11,11,12,12-tetracyano-9,10-anthraquinodimethane.

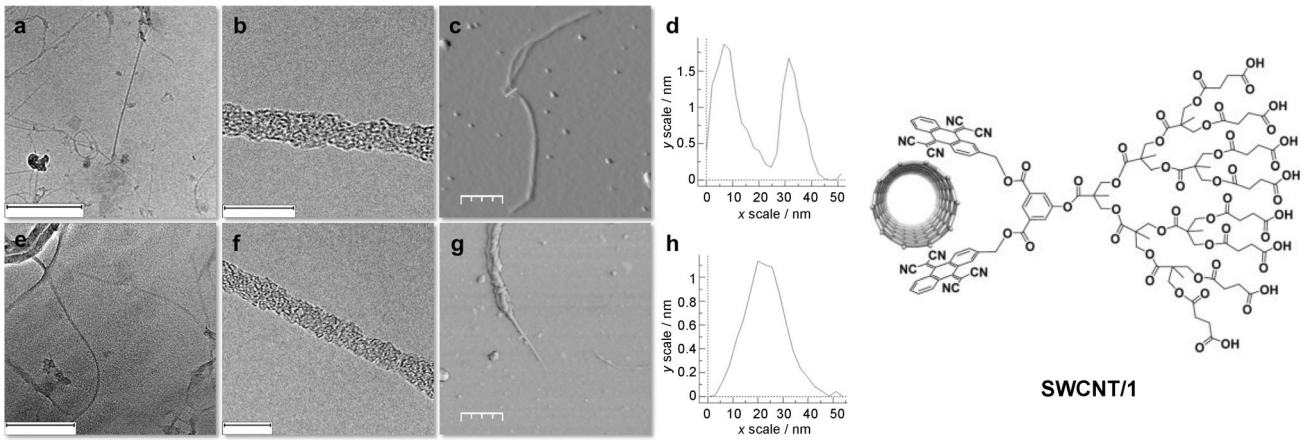

Figure 1. TEM, HRTEM, and AFM images of CoMoCAT SWCNT/**1**. a) TEM image of (6,5)/**1**; scale bar of 100 nm. b) HRTEM image of (6,5)/**1**; scale bar of 10 nm. c) AFM image of (6,5)/**1**; scale bar 140 nm. d) Height profile for the cross-section in (c). e) TEM image of (7,6)/**1**; scale bar of 100 nm. f) HRTEM image of (7,6)/**1**; scale bar of 10 nm. g) AFM image of (7,6)/**1**; scale bar 200 nm. h) Height profile for the cross-section in (g).

spectroscopic characterization of the new compounds are provided in the Supporting Information. The experimental parameters en-route towards SWCNT/**1** were optimized with respect to debundling, individualizing, and stabilizing SWCNTs. The latter are essential to shed light onto the intrinsic spectroscopic features of SWCNTs. TCAQ nanotweezers **1** (Figure 1) are soluble in aqueous media at both neutral and basic pH values. Thus, SWCNT/**1** was prepared by increasingly adding 1.2 mg of **1** to 0.5 mg of SWCNTs that were presuspended in 10 mL of a 0.1M borax solution (see details in the Supporting Information). Our procedure rendered the resulting SWCNT/**1** suspensions suitably stable for a full-fledged characterization by atomic force microscopy (AFM), transmission electron microscopy (TEM), thermogravimetric analysis (TGA) as well as Raman, steady-state, and time-resolved spectroscopies.

AFM images confirmed not only a high degree of debundling, but also the presence of **1** as amorphous material that is immobilized onto SWCNTs (Figure 1 and Figure S7). Height profiles attested, in turn, the coexistence of mostly individualized SWCNTs (1.1–1.6 nm high) that coexist with a few smaller aggregates (up to 7 nm in height). TEM measurements with mixed CoMoCAT as well as with (7,6)- and (6,5)-enriched SWCNTs further corroborated these observations (Figure 1 and Figure S7).

With different SWCNT/**1** suspensions at hand, we initially focused on establishing in situ spectroscopic signatures associated with the SCWNTs to TCAQ charge-transfer chemistry and on exploring the underlying processes. In the ground state, we note that the immobilization of **1** onto mixed CoMoCAT leads to distinct shifts of the SWCNT centered absorptions (Figure S8). For example, in the visible region, maxima evolve at 465, 515, 575, 600, 660, 740, and 860 nm that are associated with the second E_{22} electronic transitions, followed by maxima in the near-infrared region at 1015, 1055, 1160, and 1295 nm that relate to the first E_{11} electronic transitions. The corresponding E_{22} and E_{11} transitions should be compared to maxima at 450, 500, 570, 590, 650, 725, 980, 1025, 1155, and 1265 nm as they are observed for mixed CoMoCAT stabilized with sodium dodecylbenzenesulfonate (SDBS; CoMoCAT/SDBS).[15] Considering the strong electron-accepting features of TCAQ we rationalize the underlying red shifts to a redistribution of charge density and to *p*-type doping of SWCNTs. Reaggregation of SWCNTs, as an alternative cause, plays no major rule as our AFM and TEM assays infer. Just on the contrary, **1** has evolved as one of the most effective dispersant for SWCNTs. In addition, we performed similar experiments with (6,5)- and (7,6)-enriched SWCNTs. For (6,5), the maxima shift for (6,5)/SDBS[15] from 455, 570, 650, 986, and 1130 nm to 470, 580, 670, 1015, and 1180 nm for (6,5)/**1** (Figure S8). For (7,6)/**1**, maxima are found at 460, 510, 600, 665, 740, 1065, and 1170 nm relative to those seen at 455, 508, 592, 658, 732, 1026, and 1148 nm for (7,6)/SDBS (Figure S8).[15] Again, **1** effectively *p*-type dopes SWCNTs, while different degrees of aggregation are ruled out based on AFM and TEM.

Next, the fluorescence features of mixed CoMoCAT/SDBS and mixed CoMoCAT/**1** were tested. In particular, mixed CoMoCAT/SDBS displays E_{11} fluorescence maxima at 965, 1032, 1125, and 1250 nm, which are attributed to (6,5), (7,5), (7,6), and (8,7) SWCNTs (Figure S9). The fluorescent features mirror the E_{11} transitions recorded in the ground-state absorption. In turn, mixed CoMoCAT/**1** reveals an energetic shift. In particular, the E_{11} fluorescence maxima evolve at 1005, 1065, 1165, 1295, and 1445 nm (Figure S9). A redistribution of electron density from the electron-donating SWCNTs to TCAQ is likely to be responsible for the underlying shifts. Contrasting the fluorescence of the SWCNT/**1** with that of SWCNT/SDBS at equal absorbances at the excitation wavelength sheds light onto the mutual interactions by either radiative or nonradiative decays. Examination of the fluorescence intensities of mixed CoMoCAT/SDBS and mixed CoMoCAT/**1** prompts to nearly 90% quenching. Hereby, the medium energy transitions (1165 nm (7,6)) are stronger quenched than the lower (1005 nm (6,5) and 1065 nm (7,5)) and higher energy transitions (1295 nm (8,7) and 1445 nm). Accordingly, we imply the occurrence of nonradiative singlet excited-state deactivations. Nevertheless,

(7,6) SWCNTs are most heavily involved in these excited-state interactions. Further corroboration for the aforementioned came from fluorescence imaging of (6,5)-enriched SWCNTs. (6,5)/SDBS exhibit maxima at 965, 1032, and 1125 nm, while the maxima for (6,5)/**1** are at 1005, 1065, and 1165 nm (Figure S10). Again, the quenching is as strong as 95% for (7,6) SWCNTs and, as such, similar to that observed for mixed CoMoCAT. Likewise, for the (7,6)-enriched SWCNTs fluorescence maxima evolve at 970, 1032, 1125, and 1255 nm in the presence of SDBS, which shift in the presence of **1** to 980, 1065, 1165, 1295, and 1445 nm (Figure 2).[16]

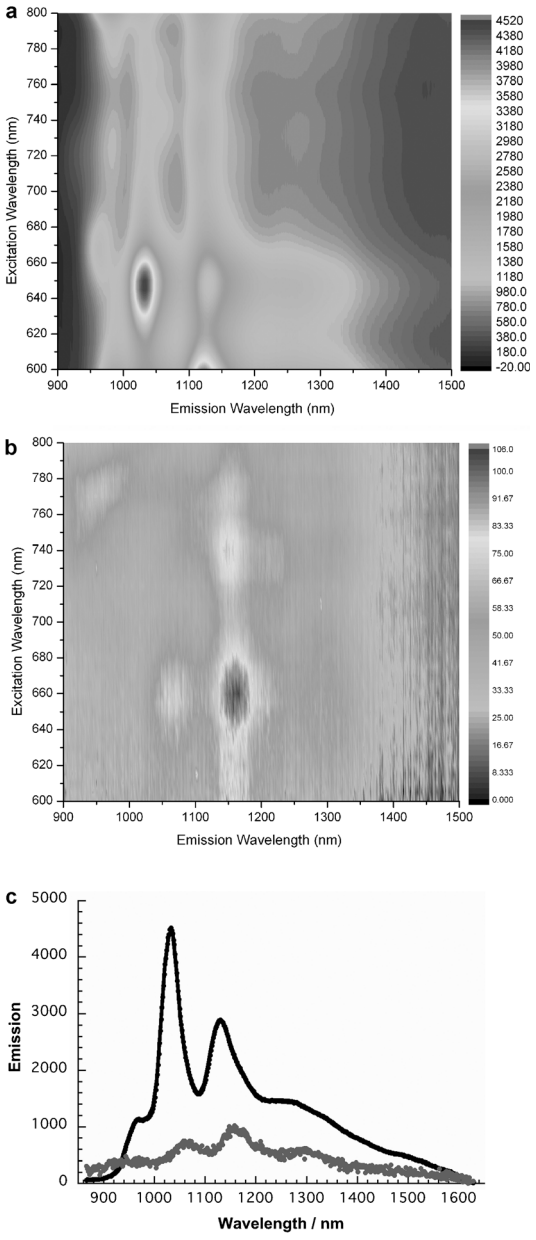

Figure 2. Steady-State fluorescence spectra of CoMoCAT SWCNT/SDBS and CoMoCAT SWCNT/**1**. a) 3D steady-state fluorescence spectra of (7,6)/SDBS in D_2O. b) 3D steady-state fluorescence spectra of (7,6)/**1** in D_2O. c) Comparison of the NIR fluorescence spectra of (7,6)/SDBS (black spectrum) and (7,6)/**1** (gray spectrum) amplified by a factor of 10 in D_2O (650 nm excitation).

To investigate the reversibility of immobilizing **1** onto SWCNTs we titrated SWCNT/**1** with SDBS and monitored the changes associated with converting SWCNT/**1** to SWCNT/SDBS by absorption and fluorescence.[7,17] Only a slight intensification of the fluorescence intensity (5%) and a minor hypsochromic shift in terms of absorption and fluorescence was detected for mixed CoMoCAT/**1**, (7,6)/**1**, and (6,5)/**1** at a SDBS concentration of 0.2 g mL^{-1} and applying 10 minutes of ultrasound. Next, we carried out TGA measurements to deduce the relative ratio between SWCNT and **1** (Figure S11). While **1** shows a two-stage decomposition with an overall 81% weight loss at 510 °C, pristine (6,5) SWCNTs reveal in the same temperature range only a minor weight loss of 4%. For (6,5)/**1** a decomposition pattern evolves that is similar to that of **1** and a weight loss of 33% at 510 °C. Accordingly, we conclude that on average one molecule of **1** is immobilized per 360 SWCNT carbon atoms.

Insights into the electronic interactions of SWCNT/**1** and SWCNT doping came from Raman experiments. For all of the SWCNT/**1** samples the G- and D*-modes are seen at 1592 and 2556 cm^{-1}, respectively (Figure 3). Notable are shifts relative to SWCNT/SDBS. In the latter, the corresponding modes

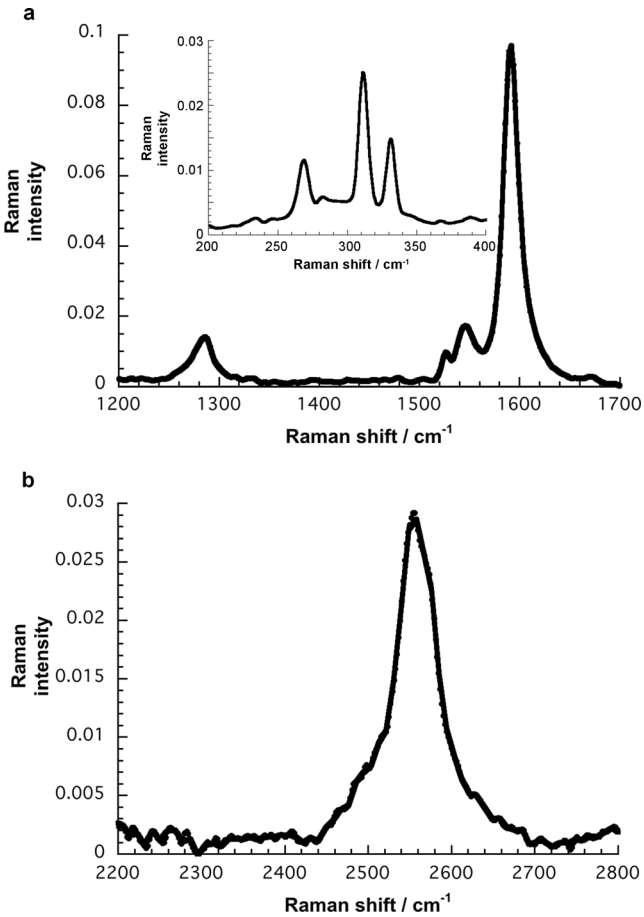

Figure 3. Raman characterization of CoMoCAT SWCNT/**1**. a) Raman spectrum of (6,5)/**1** in D_2O suspension with focus on RBM-, D-, and G-modes. b) Raman spectrum of (6,5)/**1** in D_2O suspension with focus on D*-mode (1064 nm excitation).

evolve at 1590 and 2548 cm^{-1}. No doubt, shifts of 2 and 8 cm^{-1} reflect the *p*-type SWCNT doping upon interacting with **1**.[18]

For mixed CoMoCAT, which were stabilized with SDBS, we noted in complementary femtosecond pump probe experiments negative differential absorption changes that match the ground state features. Immediately (i.e., 1 ps) upon femtosecond excitation, minima in the visible range at 570, 590, 650, and 725 nm and minima in the near-infrared range at 980 and 1130 nm evolve, which correspond to a change of oscillator strength in SWCNTs (Figure S12). In addition, shoulders at 1030 and 1270 nm followed by a maximum at 1465 nm were seen to develop. The decay of the mixed SWCNT/SDBS excited states is fast and multiexponential. In fact, within 750 ps upon photoexcitation all of the features decay. Two lifetimes of 0.6 ± 0.2 and 68 ± 10 ps dominate the dynamics that lead to the recovery of the ground state. In line with previous investigations,[11] the formation of new maxima (i.e., featuring positive differential absorption changes) at 485, 530, 610, 1065, 1215, and 1390 nm is associated with the transformation of the short-lived transient into the long-lived species before it decays entirely.

In the corresponding experiments with the (6,5)- and (7,6)-enriched SWCNTs the minima are located at 460, 575, 650, 980, and 1130 nm and 460, 510, 590, 650, 1030, and 1140 nm for (6,5)/SDBS and (7,6)/SDBS, respectively (Figure S13). These transients decay with approximately 1.5 ± 0.2 ps into maxima at 485, 610, 745, 1065, 1215, and 1420 nm for (6,5)/SDBS as well as maxima at 480, 530, 760, 1065 and 1430 nm for (7,6)/SDBS. Importantly, the same maxima are seen in the aforementioned experiments with mixed CoMoCAT. In fact, even the lifetimes are comparable with values of 80 ± 15 ps (i.e., (6,5)/SDBS) and 60 ± 5 ps (i.e., (7,6)/SDBS).

Upon immobilization of TCAQ (**1**), minima at 475, 520, 575, 600, 652, 740, 1065, and 1155 nm as well as shoulders at 1020 and 1300 nm are discernable in femtosecond pump probe experiments with mixed CoMoCAT (Figure S14). Again, these are exact matches to the ground-state absorption of mixed CoMoCAT/**1** (Figure S8). Importantly, the aforementioned attest the successful excitation of SWCNTs despite the presence of TCAQ. However, within the time window of a few picoseconds new transient features are seen to develop as a consequence of a rapid SWCNT/**1** excited-state decay.[19] Notable is, however, the lack of evidence for the long-lived species seen of mixed CoMoCAT/SDBS with its fingerprints at 1065, 1215, and 1357 nm. Instead, the visible region is dominated by maxima at 490, 540, 615, 845, and 900 nm. Pulse radiolytic reduction of TCAQ gives rise to a shoulder at 545 nm and a maximum at 610 nm in the visible region (Figure S15). In the near-infrared region a shoulder at 1005 nm and minima at 1030 and 1145 nm are discernable that are accompanied by a 1490 nm maximum. Of particular relevance is that spectroelectrochemical oxidation of mixed CoMoCAT/SDBS generates a similar absorption pattern, that is, a bleaching at 985 nm and a positive absorption in the red part of the spectrum (i.e., >1030 nm).[8] In light of the aforementioned, we postulate that the selective excitation of SWCNT/**1**, in which sizeable shifts of electron density prevail in the ground state, is followed by a full separation of charges, namely reduction of TCAQ and oxidation of SWCNTs. From multiwavelength analyses we derived the charge separation and charge recombination dynamics as 1.4 ± 0.2 and 80 ± 10 ps, respectively.

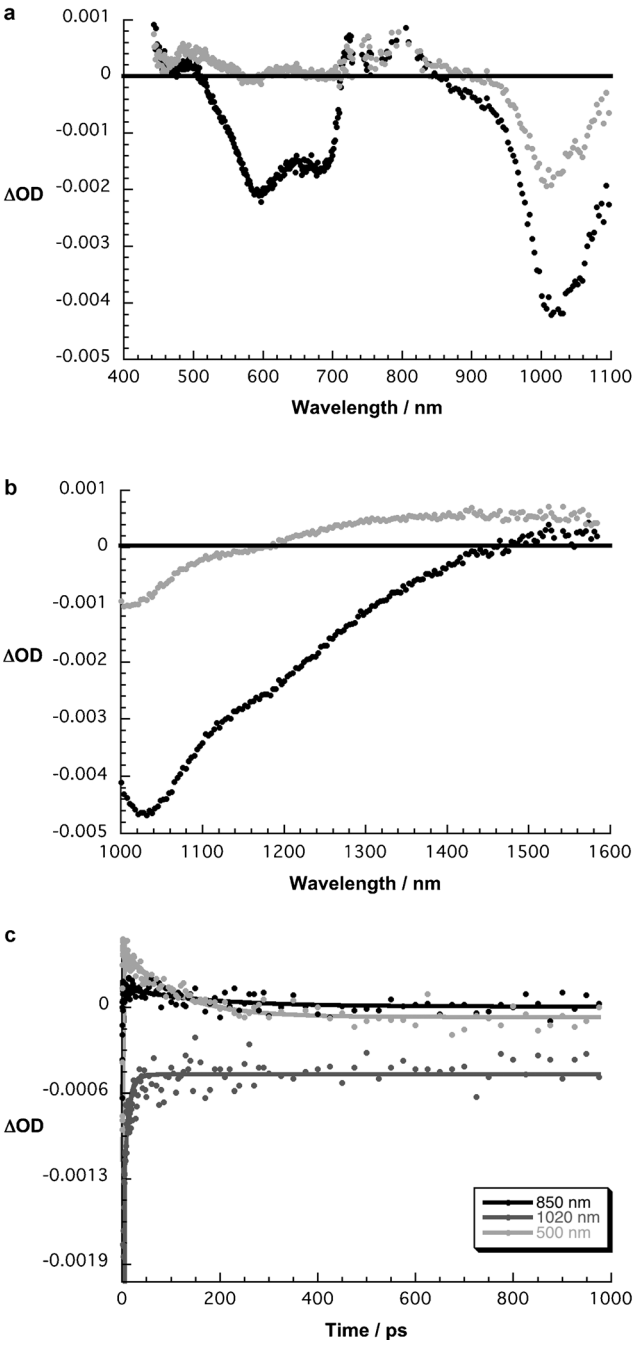

Figure 4. Photophysics of (6,5)-enriched CoMoCAT SWCNT/**1**. a) Differential absorption spectra (visible and near-infrared) obtained upon femtosecond pump–probe experiments (387 nm) of (6,5)/**1** in D_2O with time delays of 0.8 (black spectrum) and 2.3 ps (gray spectrum) at room temperature. b) Differential absorption spectra (extended near-infrared) obtained upon femtosecond pump–probe experiments (387 nm) of (6,5)/**1** in D_2O with time delays of 0.8 (black spectrum) and 2.3 ps (gray spectrum) at room temperature. c) Time–absorption profiles of the spectra shown in the upper and central parts at 500 (gray spectrum), 850 (black spectrum), and 1020 nm (gray spectrum) monitoring the charge transfer.[20]

As a complement to the aforementioned we turned to (6,5)- and (7,6)-enriched SWCNTs (Figure 4 and Figure S16). Because of the SWCNT enrichment fewer minima, that is, at 480, 525, 605, 680, 1065, and 1155 nm, evolve for (7,6)/**1** than for the mixed CoMoCAT/**1** (Figure S16). In line with the size quantization, the corresponding minima for (6,5)/**1** are blue-shifted to 470, 595, and 675 nm in the visible and to 1020 nm in the near-infrared when compared to (7,6)/**1**. In both cases, charge separation leads within 1.0 ps to the reduction of TCAQ with its 490, 540, and 615 nm features. Evidence for the oxidation of SWCNTs differs between (7,6)/**1** and (6,5)/**1** with minima at 1030/1045 and 1005 nm and maxima at 1480 and 1400 nm, respectively. The relative position of the minima and maxima are in excellent agreement. A trend is seen in the charge recombination dynamics with 90 ± 10 ps for (7,6)/**1** and 130 ± 20 ps for (6,5)/**1**. In other words, larger band gaps and higher oxidation potentials in (6,5) SWCNTs are beneficial to stabilize the charge-separated state.[21]

In conclusion, we have documented the resourcefulness of novel electron–acceptor TCAQ water-soluble nanotweezers **1** to *p*-type dope SWCNTs and to form exceptionally stable *n*-/*p*-type dispersions with SWCNTs in aqueous media. A state of the art photophysical investigation supports the notion that a dark charge-transfer state in SWCNT/**1** transforms upon photoexcitation into a fully charge-separated state. When probing enriched samples of (6,5) and (7,6) SWCNTs, benefits for a more stable charge separated state, that is, 130 ± 20 ps for (6,5)/**1** and 90 ± 10 ps for (7,6)/**1**, emerged from larger band gaps (1.15 versus 1.05 eV) and higher oxidation potentials (0.64 versus 0.5 V). Our investigations infer charge-separation and charge-recombination dynamics in SWCNT-based electron donor–acceptor nanohybrids that are, like in analogous fullerenes, located in the Marcus-normal and in the Marcus-inverted region, respectively.[22] The latter is of great interest in devising SWCNT-based electron donor–acceptor nanohybrids that allow the storage of a maximum of energy.

Received: May 10, 2013
Revised: July 2, 2013
Published online: August 9, 2013

Keywords: carbon nanotubes · charge transfer · chemical doping · donor–acceptor systems · molecular tweezers

[1] S. Iijima, *Nature* **1991**, *354*, 56 – 58.
[2] D. M. Guldi, N. Martín, *Carbon nanotubes and related structures*, Wiley-VCH, Weinheim, **2010**.
[3] T. Akasaka, F. Wudl, S. Nagase, *Chemistry of nanocarbons*, Wiley, Chichester, **2010**.
[4] a) G. Magadur, J.-S. Lauret, G. Charron, F. Bouanis, E. Norman, V. Huc, C.-S. Cojocaru, S. Gómez-Coca, E. Ruiz, T. Mallah, *J. Am. Chem. Soc.* **2012**, *134*, 7896 – 7901; b) S. Wang, Q. Zeng, L. Yang, Z. Zhang, Z. Wang, T. Pei, L. Ding, X. Liang, M. Gao, Y. Li, L.-M. Peng, *Nano Lett.* **2011**, *11*, 23 – 29; c) J. M. Lee, J. S. Park, S. H. Lee, H. Kim, S. Yoo, S. O. Kim, *Adv. Mater.* **2011**, *23*, 629 – 633; d) F. M. Toma, A. Sartorel, M. Iurlo, M. Carraro, P. Parisse, C. Maccato, S. Rapino, B. Rodríguez-González, H. Amenitsch, T. Da Ros, L Casalis, A. Goldoni, M. Marcaccio, G. Scorrano, G. Scoles, F. Paolucci, M. Prato, M. Bonchio, *Nat. Chem.* **2010**, *2*, 826 – 831; e) B. Esser, J. M. Scnorr, T. M. Swager, *Angew. Chem.* **2012**, *124*, 5851 – 5855; *Angew. Chem. Int. Ed.* **2012**, *51*, 5752 – 5756; f) M. C. Rosamond, A. M. Martin, A. Ayesh, A. Al Ghaferi, A. J. Gallant, M. F. Mabrook, D. A. Zeze, *Appl. Phys. Lett.* **2012**, *100*, 023302; g) W. Guo, C. Liu, X. Sun, Z. Yang, H. G. Kia, H. Peng, *J. Mater. Chem.* **2012**, *22*, 903 – 908.
[5] S. A. Hodge, M. K. Bayazit, K. S. Coleman, M. S. P. Shaffer, *Chem. Soc. Rev.* **2012**, *41*, 4409 – 4429.
[6] N. Martín, J. F. Nierengarten, *Supramolecular chemistry of fullerenes and carbon nanotubes*, Wiley-VCH, Weinheim, **2012**.
[7] C. Ehli, C. Oelsner, D. M. Guldi, A. Mateo-Alonso, M. Prato, C. Schmidt, C. Backes, F. Hauke, A. Hirsch, *Nat. Chem.* **2009**, *1*, 243 – 249.
[8] C. Oelsner, C. Schmidt, F. Hauke, M. Prato, A. Hirsch, D. M. Guldi, *J. Am. Chem. Soc.* **2011**, *133*, 4580 – 4586. The overall red-shifts are due to interactions between SWCNTs with **1**.
[9] J. Bartelmess, C. Ehli, J. J. Cid, M. García-Iglesias, P. Vázquez, T. Torres, D. M. Guldi, *J. Mater. Chem.* **2011**, *21*, 8014 – 8020.
[10] J. Bartelmess, C. Ehli, J. J. Cid, M. García-Iglesias, P. Vázquez, T. Torres, D. M. Guldi, *Chem. Sci.* **2011**, *2*, 652 – 660.
[11] a) C. Romero-Nieto, R. García, M. A. Herranz, C. Ehli, M. Ruppert, A. Hirsch, D. M. Guldi, N. Martín, *J. Am. Chem. Soc.* **2012**, *134*, 9183 – 9192; b) F. G. Brunetti, C. Romero-Nieto, J. López-Andarias, C. Atienza, J. L. López, D. M. Guldi, N. Martín, *Angew. Chem.* **2013**, *125*, 2236 – 2240; *Angew. Chem. Int. Ed.* **2013**, *52*, 2180 – 2184.
[12] N. Martin, R. Behnisch, M. Hanack, *J. Org. Chem.* **1989**, *54*, 2563 – 2568.
[13] E. Ortí, R. Viruela, P. M. Viruela, *J. Phys. Chem.* **1996**, *100*, 6138 – 6146.
[14] The supramolecular interaction of TCAQ nanotweezers with C_{60} was previously investigated: E. M. Pérez, A. L. Capodilupo, G. Fernández, L. Sánchez, P. M. Viruela, R. Viruela, E. Ortí, M. Bietti, N. Martín, *Chem. Commun.* **2008**, 4567 – 4569.
[15] SWCNT/SDBS reference solutions were prepared from the same nanotubes batches that were employed in the preparation of the SWCNT/**1** nanohybrids.
[16] Here, it is, however, the fluorescence of (7,5) SWCNTs that is strongest quenched.
[17] U. Hahn, S. Engmann, C. Oelsner, C. Ehli, D. M. Guldi, T. Torres, *J. Am. Chem. Soc.* **2010**, *132*, 6392 – 6401.
[18] R. Voggu, C. S. Rout, A. D. Franklin, T. S. Fisher, C. N. R. Rao, *J. Phys. Chem. C* **2008**, *112*, 13053 – 13056.
[19] In reference experiments with **1**, the differential absorption changes are governed by a 600 nm maximum in the visible and a 1080 nm maximum in the near-infrared, which decay within 2000 ps.
[20] The noted differences in intensities between the visible/near-infrared and the extended near-infrared are due to different white light sources.
[21] From a comparison of the charge recombination dynamics we conclude that the mixture of SWCNT/**1** contains mainly (7,6)/**1**.
[22] a) D. M. Guldi, M. Prato, *Acc. Chem. Res.* **2000**, *33*, 695 – 703; b) D. M. Guldi, K.-D. Asmus, *J. Am. Chem. Soc.* **1997**, *119*, 5744 – 5745.

